Killing Mechanism of Stable *N*-Halamine Cross-Linked Polymethacrylamide Nanoparticles That Selectively Target Bacteria

Michal Natan,[†,§,⊥] Ori Gutman,[‡,§,⊥] Ronit Lavi,[‡] Shlomo Margel,[*,‡,§] and Ehud Banin[*,†,§]

[†]The Mina and Everard Goodman Faculty of Life Sciences, [‡]The Department of Chemistry, and [§]The Institute for Advanced Materials and Nanotechnology, Bar-Ilan University, Ramat-Gan 52900, Israel. [⊥]These authors contributed equally to this work.

ABSTRACT Increased resistance of bacteria to disinfection and antimicrobial treatment poses a serious public health threat worldwide. This has prompted the search for agents that can inhibit both bacterial growth and withstand harsh conditions (*e.g.*, high organic loads). In the current study, *N*-halamine-derivatized cross-linked polymethacrylamide nanoparticles (NPs) were synthesized by co-polymerization of the monomer methacrylamide (MAA) and the cross-linker monomer *N*,*N*-methylenebis(acrylamide) (MBAA) and were subsequently loaded with oxidative chlorine using sodium hypochlorite (NaOCl). The chlorinated NPs demonstrated remarkable stability and durability to organic reagents and to repetitive bacterial loading cycles as compared with the common disinfectant NaOCl (bleach), which was extremely labile under these conditions. The antibacterial mechanism of the cross-linked P(MAA-MBAA)-Cl NPs was found to involve generation of reactive oxygen species (ROS) only upon exposure to organic media. Importantly, ROS were not generated upon suspension in water, revealing that the mode of action is target-specific. Further, a unique and specific interaction of the chlorinated NPs with *Staphylococcus aureus* was discovered, whereby these microorganisms were all specifically targeted and marked for destruction. This bacterial encircling was achieved without using a targeting module (*e.g.*, an antibody or a ligand) and represents a highly beneficial, natural property of the P(MAA-MBAA)-Cl nanostructures. Our findings provide insights into the mechanism of action of P(MAA-MBAA)-Cl NPs and demonstrate the superior efficacy of the NPs over bleach (*i.e.*, stability, specificity, and targeting). This work underscores the potential of developing sustainable P(MAA-MBAA)-Cl NP-based devices for inhibiting bacterial colonization and growth.

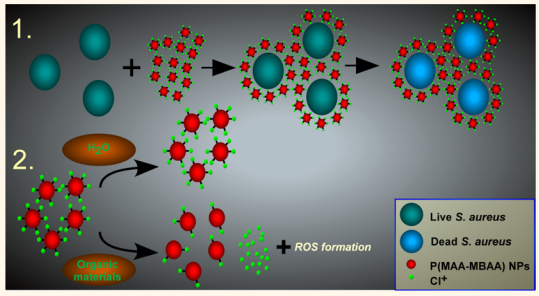

KEYWORDS: nanoparticles · bacteria · targeting · antibacterial · stable · reactive oxygen species · controlled release

The re-emergence of bacterial infections as well as the increased incidence of antimicrobial resistance among pathogenic bacteria constitute one of the paramount challenges facing humanity today, presenting a serious public health threat worldwide. The threat is particularly worrying in light of the few antimicrobial agents expected to enter the market in the near future.[1−3] In the United States alone, around 2 million people acquire bacterial infections annually, resulting in 90 000 deaths each year.[4] Indeed, the Center for Disease Control and Prevention has recently issued an assessment that we are very close to entering the "post-antibiotic era".[5] This highlights the need to develop novel antimicrobials and find innovative and creative solutions to inhibit bacterial growth.

New materials exhibiting antimicrobial properties have been developed over the past decade.[6,7] Among these agents, *N*-halamine compounds that contain one or more nitrogen−halogen covalent bonds are attracting growing interest as they excel as antimicrobials. Moreover, *N*-halamine agents have long-term stability in aqueous solutions, are weakly toxic and relatively cheap, and can easily be regenerated to carry halogens.[8,9] All of these properties have made *N*-halamine compounds particularly attractive as food and water disinfectants.[10,11]

One promising approach to combating bacteria is based on nanotechnology-tailored

* Address corresponds to ehud.banin@biu.ac.il, shlomo.margel@mail.biu.ac.il.

Received for review August 17, 2014 and accepted January 20, 2015.

Published online January 20, 2015
10.1021/nn507168x

agents. Nanoparticles (NPs) have peculiar and well-defined properties that distinguish them from their bulk chemical counterparts, for example, large surface area to volume ratio. The latter enhances the interaction of NPs with a given microbe due to a higher number of functional sites. Probably the most studied antibacterial NPs are made of silver.[12] Several studies have shown that silver NPs have enhanced antimicrobial activity compared to silver ions.[13,14] Recently, it was reported that carbon nanoscrolls filled with silver NPs exhibit lengthened antifungal activities due to the controlled release of the silver ions.[15] However, lately, regulatory agencies have been expressing less enthusiasm toward nano-Ag due to its possible cytotoxicity.[16−18] Other metals such as gold, metal fluorides, and metal oxide NPs have also been shown by us and others to have strong antimicrobial activity against a wide range of pathogenic microorganisms.[19−24] Additionally, our group has recently reported the sonochemical synthesis of a Zn- doped CuO composite (*i.e.*, ZnCuO), which demonstrated antibacterial properties stronger than the ones detected with just CuO or ZnO NPs.[25] Carbon nanotubes are another example as highly purified single-walled carbon nanotubes were also shown to exhibit strong antimicrobial activity.[26] Nevertheless, these mentioned NPs and other disinfection agents are non-rechargeable, susceptible to organic materials, and thus only provide short-term protection.

Recently, we sought to combine the advantages of *N*-halamine compounds and nanotechnology-driven agents. To this end, we fabricated novel recyclable *N*-halamine-derivatized cross-linked polymethacrylamide NPs *via* surfactant-free dispersion copolymerization of methacrylamide (MAA) and the cross-linking monomer *N*,*N*-methylenebis(acrylamide) (MBAA) in an aqueous continuous phase, followed by chlorination *via* NaOCl.[27] These chloramine-derivatized NPs were found to be extremely potent against *Escherichia coli* and *Staphylococcus aureus* as well as against multidrug-resistant bacteria, establishing the efficacy of this newly synthesized material.[27] In the current study, we further characterized the antibacterial potential of P(MAA-MBAA)-Cl NPs in comparison to NaOCl (bleach), one of the most widely used disinfectants in medical, industrial, and domestic settings. We show that the nanoscale P(MAA-MBAA)-Cl retains potent antibacterial activity even after exposure to organic materials and repetitive bacterial loading cycles as compared to bleach, which is highly labile under these conditions, losing its biocidal activity rapidly. We also investigated the mechanism whereby the P(MAA-MBAA)-Cl NPs kill bacteria by monitoring generation of reactive oxygen species (ROS), bacterial interaction, and the ability to inflict morphological changes. Our results support the utility of P(MAA-MBAA)-Cl NPs as potent antimicrobials with various environmental and biomedical applications, as the NPs withstand harsh organic conditions.

RESULTS AND DISCUSSION

Characterization of the Chlorinated and Non-chlorinated P(MAA-MBAA) NPs. P(MAA-MBAA) NPs were synthesized as described in the Methods section. Solid-state NMR was conducted as a complementary analysis to the characterization assays conducted previously[27] to monitor the polymerization process and distinguish between the chlorinated and non-chlorinated P(MAA-MBAA) NPs.

The P(MAA-MBAA) NPs were verified by the disappearance of the vinylic proton peaks at 5.12 and 5.91 ppm and the appearance of broad peaks of the polymer aliphatic protons at 1−3.5 ppm. Additionally, new cross-linker methylene protons appeared at 4.77 ppm. The chlorination was also verified by ^{1}H NMR. The amide proton peak at 7−9 ppm disappeared when H replaced Cl, and the methylene proton peak was shifted to 5.5 ppm because of the chlorination of the methylene substitutions. X-ray diffraction (XRD) characterization presented in Figure 1 demonstrates the XRD patterns of the MAA and MBAA monomers *versus* the P(MAA-MBAA) NPs and the chlorinated ones. The XRD measurements on the MAA and MBAA monomer powders display clear sharp and narrow diffraction peaks, typically observed for crystalline materials (Figure 1A,B), while the X-ray powder diffraction of the NPs revealed very poor diffraction patterns, pointing to the amorphous nature of the NPs (Figure 1C,D).

The zeta-potential was also evaluated for the NPs as it may affect their stability. The zeta-potential was found to be negative: −11.3 and −12.72 mV for the chlorinated NPs and their non-chlorinated counterparts, respectively. Finally, the P(MAA-MBAA)-Cl NPs were also imaged using cryogenic transmission electron microscopy (cryo-TEM) as this reveals their dry size (Supporting Information, Figure S1) which was estimated to be between 5 and 9 nm.

P(MAA-MBAA)-Cl NPs Withstand Repeated Loading of Bacteria and Organic Materials. We began by characterizing the bactericidal potential of P(MAA-MBAA)-Cl NPs relative to the soluble non-nanometric *N*-halamine polymer MAA-Cl (*i.e.*, PMAA-Cl) and to NaOCl, the chemical that was used to load the P(MAA-MBAA)-NPs with oxidative Cl (see Methods section) and is the active ingredient of household bleach, one of the most commonly used disinfectants in the world.[28] All three reagents release Cl^{+} that kills bacteria, and the oxidative chlorine concentrations used were 11 and 8 mM. As presented in Table 1, the chlorinated NPs and NaOCl killed both *E. coli* and *S. aureus*, two common bacterial pathogens representing Gram-negative and Gram-positive bacteria, respectively, while the PMAA-Cl was much less effective and killed only *S. aureus*. These results clearly show that P(MAA-MBAA)-Cl NPs and NaOCl are more

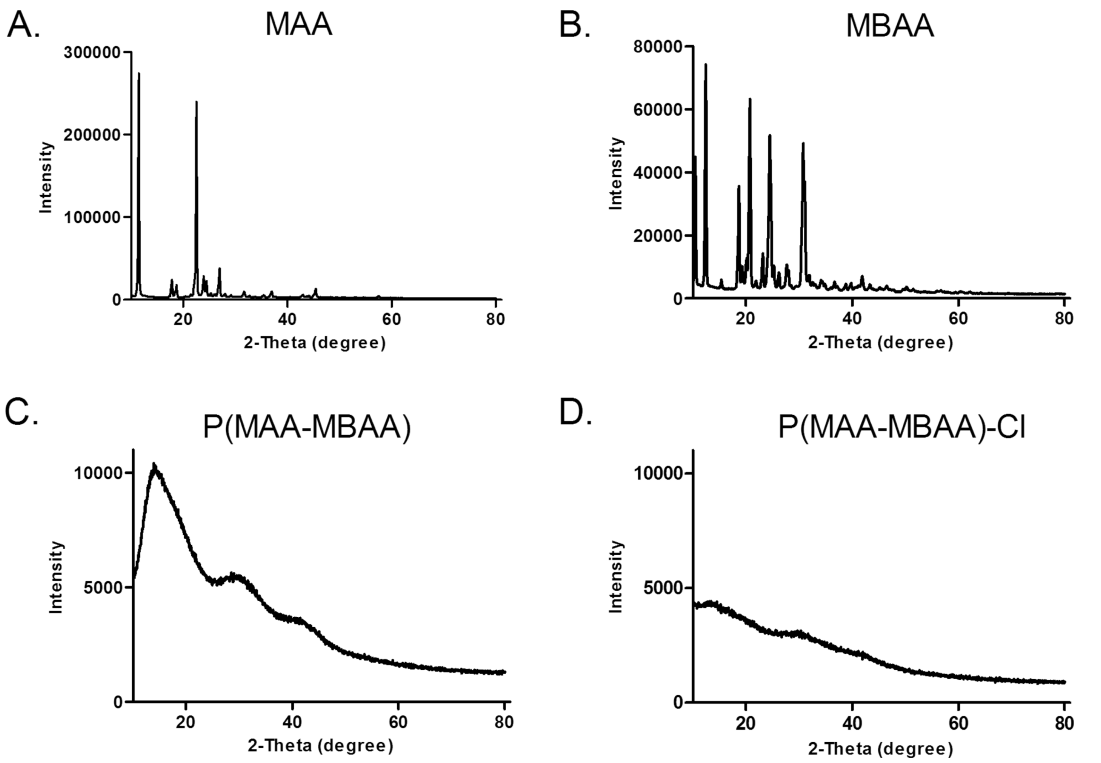

Figure 1. XRD patterns of the monomers MAA (A), MBAA (B), and the polymerized NPs P(MAA-MBAA) (C) and the charged ones (D).

TABLE 1. Antibacterial Activity of P(MAA-MBAA)-Cl NPs, PMAA-Cl, and NaOCl against *E. coli* and *S. aureus*

reagent name	*E. coli*	*S. aureus*
P(MAA-MBAA)-Cl NPs (11 mM)	total kill	total kill
P(MAA-MBAA)-Cl NPs (8 mM)	total kill	total kill
PMAA-Cl (11 mM)	6 log (out of 10)	total kill
PMAA-Cl (8 mM)	no killing	total kill
NaOCl (11 mM)	total kill	total kill
NaOCl (8 mM)	total kill	total kill

effective than the non-nanometric PMAA-Cl, and we continued comparing the antibacterial activity of these two materials in the current study.

Our next step was to determine the minimum inhibitory concentration (MIC) of the two agents. Briefly, *E. coli* and *S. aureus* were exposed to serial dilutions of either P(MAA-MBAA)-Cl NPs (aqueous dispersion) or NaOCl. The MIC of the two reagents was found to be the same, 5.6 mM oxidative Cl, for both *E. coli* and *S. aureus*. Notably, bacteria exposed to non-chlorinated P(MAA-MBAA) NPs did not exhibit growth arrest and behaved like untreated bacteria, which is in accordance with our previous report.[27]

Next, we tested the capability of chlorinated NPs *versus* NaOCl to withstand repetitive cycles of bacterial exposure. To this end, both *E. coli* and *S. aureus* were incubated with either NaOCl or the chlorinated NPs. This concentration was applied in all the experiments, unless indicated otherwise. Every hour, a sample was

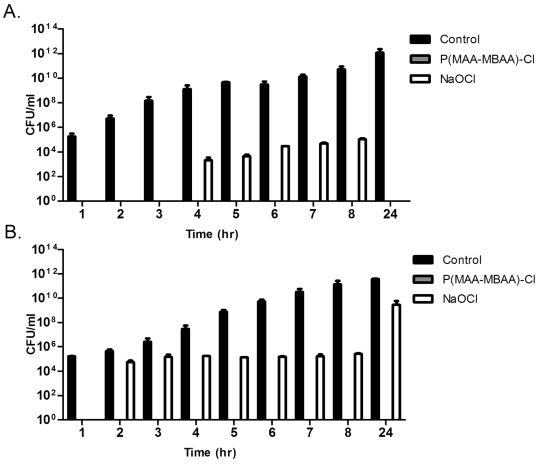

Figure 2. P(MAA-MBAA)-Cl NPs and NaOCl withstand repetitive bacterial loading cycles. (A) *E. coli* or (B) *S. aureus* were treated with either P(MAA-MBAA)-Cl NPs, NaOCl, or were untreated. Every hour, aliquots were removed from each sample and plated on agar plates. In parallel, 10^5 CFU/mL of freshly prepared bacteria was added. After the eighth loading cycle, the tubes were left in the shaker and samples taken the following day. Error bars represent the standard deviation of three independent experiments. It is important to note that, because the P(MAA-MBAA)-Cl was able to kill all the bacteria at all the indicated time points, the gray bars are not shown in the graph.

taken from each tube and plated on agar plates, and in parallel, 10^5 colony-forming units (CFU)/mL of freshly prepared bacteria was added. In total, 8 bacterial loading cycles were conducted. As presented in Figure 2, the P(MAA-MBAA)-Cl NPs retained activity

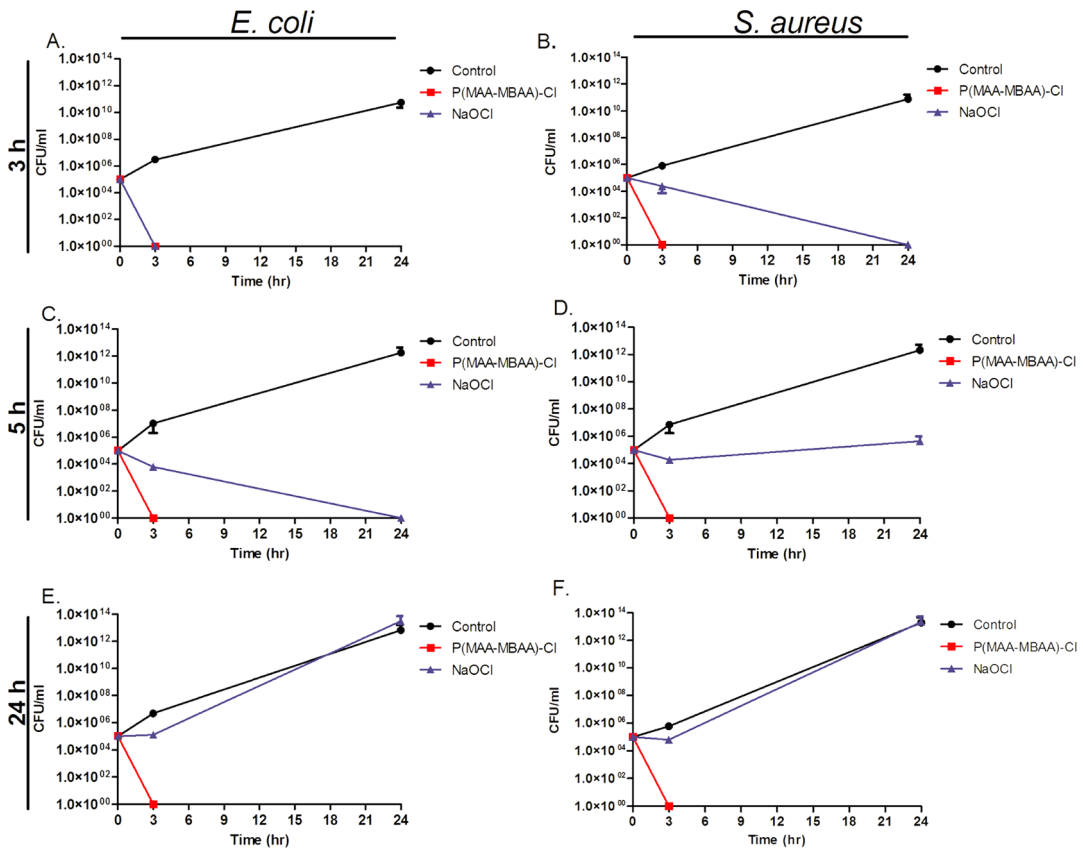

Figure 3. Short-term stability of P(MAA-MBAA)-Cl NPs *versus* NaOCl to organic material. *E. coli* (A,C,E) or *S. aureus* (B,D,F) were added to LB media that had been preincubated with either P(MAA-MBAA)-Cl NPs, NaOCl, or left untreated for 3 h (A,B), 5 h (C,D) or 24 h (E,F). Aliquots were removed after a further 3 or 24 h incubation and plated on agar plates to determine bacterial viability. Error bars indicate the standard deviation of three independent experiments.

throughout the experiment, eradicating both *E. coli* and *S. aureus*. In contrast, NaOCl was no longer able to promote bacterial killing from cycle 4 for *E. coli* and from cycle 2 for *S. aureus*. It is important to note that the quantity of bacteria exposed to bleach throughout the loading cycles did not reach the concentration of bacteria residing in the control test tube (*i.e.*, untreated bacteria) (Figure 2), suggesting that the bactericidal activity of bleach during this short incubation has been hampered. To investigate this premise, we checked the viability of bacteria sampled following an overnight incubation. After a longer exposure time to NaOCl, there were no viable *E. coli* bacteria, which suggests that given enough time bleach still managed to kill the bacteria, whereas the *S. aureus* bacteria were able to overcome the growth inhibitory affect observed following the short exposure. These data demonstrate that *S. aureus* bacteria are more resistant to bleach than *E. coli*. Importantly, after an overnight incubation with P(MAA-MBAA)-Cl NPs, neither *E. coli* nor *S. aureus* bacteria were viable (Figure 2).

A limitation of inorganic halogen-based biocides, such as bleach, is that they are very corrosive and hence susceptible to organic material.[11] Our bacterial loading results indicate that P(MAA-MBAA)-Cl NPs possess the desirable property of increased stability. To examine this further, we compared the stability of chlorinated NPs *versus* bleach in full organic media (*i.e.*, Luria–Bertani, LB). To this end, P(MAA-MBAA)-Cl NPs and NaOCl were preincubated with LB for different periods: 3, 5, or 24 h. After this initial incubation with organic media, *E. coli* or *S. aureus* bacteria were supplemented to a final concentration of 10^5 CFU/mL, and samples were taken after a further 3 or 24 h of incubation. We expected that the preincubation step would impact the efficacy of each biocide differently and the extent of impact would correlate with the length of time the samples were exposed to organic material (*i.e.*, LB) prior to addition of bacteria. As shown in Figure 3A, preincubation of NaOCl or chlorinated NPs with LB for 3 h prior to addition of *E. coli* had no impact on their bactericidal activity. However, preincubation of NaOCl with media for 3 h prior to addition of *S. aureus* did compromise its bactericidal activity, as the reagent was subsequently only capable of evincing complete killing by 24 h (Figure 3B). In contrast, preincubation of P(MAA-MBAA)-Cl NPs with media for 3 h prior to addition of *S. aureus* had no impact on its bactericidal activity, with complete killing observed after 3 h (Figure 3B). Preincubation of NaOCl with media for 5 h prior to addition of *E. coli* resulted in growth inhibition at the 3 h time point, with bacteria

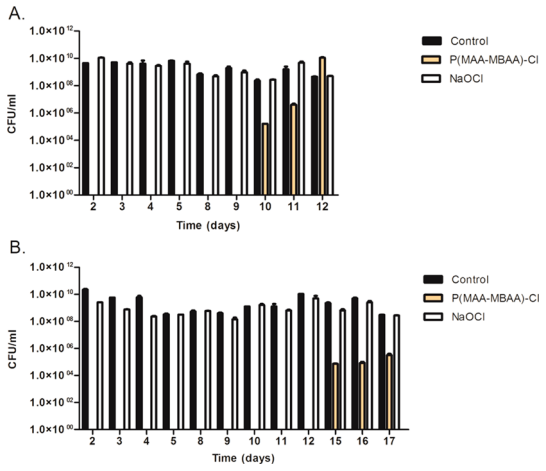

Figure 4. P(MAA-MBAA)-Cl NPs exhibit long-term activity and stability to organic materials. (A) *E. coli* or (B) *S. aureus* were treated with either P(MAA-MBAA)-Cl NPs, NaOCl, or were untreated. Each of these reagents was preincubated with LB medium for 24 h (day 1) following which 10^5 CFU/mL of the relevant bacteria was added for 24 h (day 2). Every day, aliquots were removed from each sample and plated on agar plates. In parallel, 10^5 CFU/mL of fresh bacteria was added as appropriate. Error bars represent the standard deviation of three independent experiments.

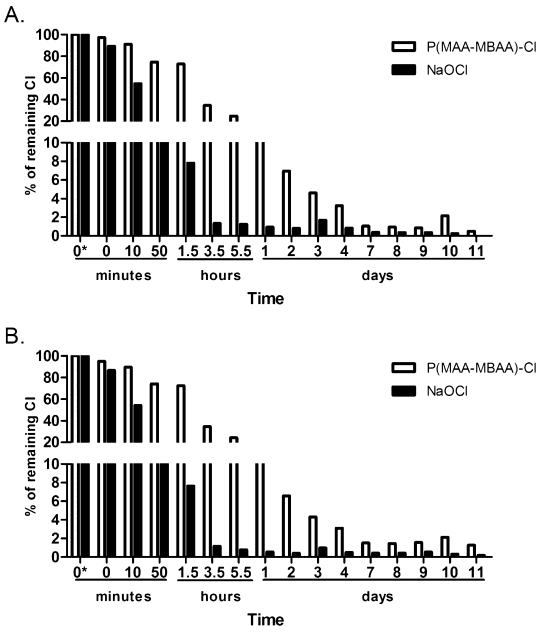

Figure 5. Kinetics of oxidative chlorine release from P(MAA-MBAA)-Cl NPs and NaOCl. Chlorinated NPs and NaOCl were incubated with LB medium, and at the stated time points, samples were taken for oxidative chlorine quenching *via* NaI. The oxidative chlorine concentrations were determined by spectrophotometry measurements at 292 nm (A) and 350 nm (B); 0* refers to the initial oxidative chlorine concentration found on either the NPs or NaOCl in water, *i.e.*, prior to addition of the organic medium.

viability reduced by almost 4 log; complete killing was evident only at 24 h (Figure 3C). The same conditions elicited growth arrest for *S. aureus* (Figure 3D), further corroborating our premise that *E. coli* is more sensitive to bleach than *S. aureus*. Remarkably, preincubation of P(MAA-MBAA)-Cl NPs with LB for 5 h prior to addition of *E. coli* or *S. aureus* did not compromise its bactericidal activity (Figure 3C,D). Finally, preincubation of NaOCl with LB for 24 h prior to addition of *E. coli* or *S. aureus* destroyed its antibacterial activity, such that the bacteria grew comparably to untreated controls (Figure 3E,F). In sharp contrast, preincubation of P(MAA-MBAA)-Cl with LB for 24 h prior to addition of *E. coli* or *S. aureus* did not compromise its bactericidal activity (Figure 3E,F). In summary, P(MAA-MBAA)-Cl NPs exhibit superior stability to organic materials when compared to bleach.

Having established that chlorinated NPs are still toxic toward bacteria despite pre-exposure to organic-rich media for 24 h, we examined the longer-term activity of P(MAA-MBAA)-Cl NPs. To this end, P(MAA-MBAA)-Cl NPs were exposed to repetitive bacterial loading cycles for up to 17 days. The chlorinated NPs retained bactericidal activity over 6 loading cycles of *E. coli* spread over 9 days, but by the seventh cycle (on the 10th day), bacterial growth was only partially attenuated, and by the ninth loading cycle (day 12), the *E. coli* grew comparably to untreated controls (Figure 4A). As for *S. aureus*, the chlorinated NPs continued killing the bacteria for nine consecutive cycles spread over 12 days, with bacterial growth only detectable on the following cycle (Figure 4B). Taken together, the data demonstrate that nanosized P(MAA-MBAA)-Cl NPs are far more stable than NaOCl when exposed to organic materials. It was of interest to check at which concentration NaOCl retained the capability to kill bacteria when the NaOCl was preincubated for 1 week with LB media. To address this, we took a sample of fresh NaOCl straight from a commercial bottle, corresponding to 0.72 M, incubated it with LB medium for 1 week, and then added bacteria. Interestingly, we found that 0.36 M of NaOCl, which is 33 times more than the concentration of the oxidative Cl bound to the NPs, is required to kill *E. coli* and *S. aureus*, with 0.18 M NaOCl ineffective (Supporting Information, Figure S2). This finding underscores the advantages of using chlorinated NPs over NaOCl, both in terms of stability and efficacy.

To investigate in more detail the stability of P(MAA-MBAA)-Cl NPs, we measured the oxidative chlorine content of the chlorinated NPs *versus* bleach after incubation in LB medium for 11 days. The oxidative chlorine concentration was determined using a spectrophotometer at 292 nm (Figure 5A) and 350 nm (Figure 5B). We observed a surge in NaOCl consumption upon exposure to LB, as the oxidative Cl release from NaOCl was very rapid, with almost 50% of the NaOCl molecules sequestered by organic substances after only 10 min of incubation in the medium (Figure 5). In contrast, approximately 90% of the NPs retained their chlorinated form, suggesting a gradual decay of the Cl^+ from the NPs as opposed to the rapid

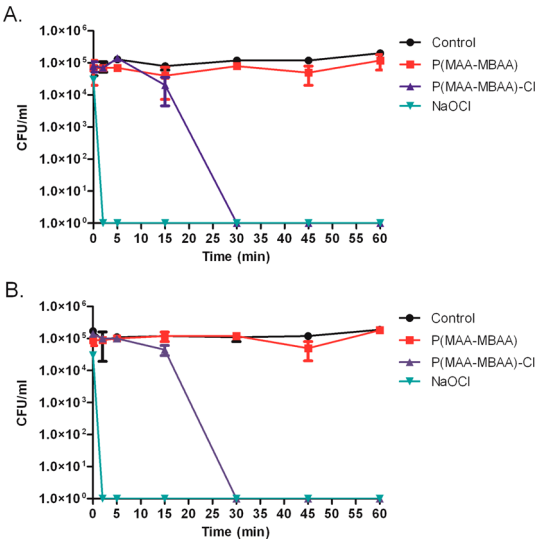

Figure 6. Killing kinetic curves of *E. coli* (A) and *S. aureus* (B) in the presence of either P(MAA-MBAA)-Cl or NaOCl. The growth curves of untreated bacteria or bacteria incubated with P(MAA-MBAA) NPs are displayed, as well. The experiments were conducted at least three independent times.

decay observed for NaOCl. Still, this amount of released Cl^+ was sufficient to induce bacterial killing even following separation of the loaded NPs as presented in Figure S3. Furthermore, after 1 day of incubation, we could barely detect Cl^+ on NaOCl, with 0.9 and 0.5% chlorinated according to measurements at 292 and 350 nm, respectively (Figure 5), whereas 12% of NPs retained Cl^+. Taken together, the data indicate that the organic materials in the medium scavenge the Cl^+ in NaOCl, compromising its activity and rendering bleach unable to kill bacteria. However, chlorinated NPs are far more stable, resist the scavenging nature of the organic material, and, hence, exhibit extended antibacterial activity under these conditions.

Given our finding that NaOCl releases reactive chlorine to the medium much more rapidly than P(MAA-MBAA)-Cl NPs, we compared the killing kinetics of these reagents in the presence of *E. coli* (Figure 6A) or *S. aureus* (Figure 6B). In line with the observed differences in the oxidative chlorine release kinetics, NaOCl acted faster, eradicating both types of bacteria within 2 min of exposure, in comparison to the chlorinated NPs that eliminated the same amount of bacteria only after 30 min (Figure 6). Importantly, bacteria suspended in water instead of LB were also eradicated faster following exposure to bleach (Supporting Information, Figure S4). Of note, the P(MAA-MBAA)-Cl NPs suspended in LB killed bacteria a bit slower compared to water, presumably due to the organic load found in LB that most likely consumed some of the Cl^+ found on the NPs. In summary, our data show that bleach exerts its antimicrobial activity faster than the NPs; however, in the long run, P(MAA-MBAA)-Cl NPs exhibit superior stability and efficacy, especially under adverse environmental conditions that contain high organic load like proteinaceous materials. Therefore, P(MAA-MBAA)-Cl NPs should be the reagent of choice.

TABLE 2. Genetically Engineered Bioluminescent Strains Employed in the Present Study[29−31]

promoter	stress sensitivity
recA	DNA damage
katG	oxidative stress (peroxides)
micF	superoxide and hyperosmotic stresses
fabA	fatty acid availability
grpE	heat shock
marR	involved in antibiotic resistance
sodA	superoxide damage and oxidative stress

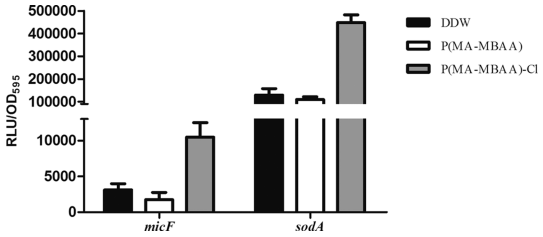

Figure 7. P(MAA-MBAA)-Cl NPs induce oxidative stress. *E. coli* strains bearing a promoter−lux fusion for oxidative stress-related genes, *i.e.*, *micF* or *sodA*, were exposed to 5.5 mM oxidative chlorine found on the P(MAA-MBAA)-Cl NPs for 8 h. Bacteria treated with either sterile water or P(MAA-MBAA) NPs served as negative controls. Gene expression was monitored by measuring luminescence. The results are presented as relative luminescence units (RLU) as a function of growth (OD595). Error bars correspond to the standard deviations of three independent experiments.

P(MAA-MBAA)-Cl NPs Exert Antimicrobial Effects *via* Oxidative Stress. To understand better the mechanism whereby the P(MAA-MBAA)-Cl nanoagents exert their toxic effects, we took advantage of biosensor *E. coli* bacteria created by Belkin and colleagues.[29−31] The genetically engineered bacteria harbor plasmid bioluminescence *lux* genes fused to specific stress response promoters and thus can be exploited to monitor activation of stress responses, such as heat shock, DNA damage, oxidative stress, and fatty acid metabolism disruption. Of all the bacteria screened (Table 2), only *E. coli* strains harboring a plasmid containing either *micF::luxCDABE* or *sodA::luxCDABE* fusion were significantly induced by the P(MAA-MBAA)-Cl NPs in comparison to bacteria treated with either water or non-chlorinated NPs (Figure 7). It is important to note that this response was observed only when a lower dose (5.5 mM) of the chlorinated NPs was applied that was not high enough to induce massive cell death but was sufficiently high to induce the bacterial defense pathways. *sodA* and *micF* are both responsive to oxidative stress, and their induction by P(MAA-MBAA)-Cl NPs likely reflects the mechanism underlying bacterial killing. Superoxide dismutase (*i.e.*, *sodA*) catalyzes the transition of superoxide (O^{2-}) to oxygen and H_2O_2,[32] and then catalase and peroxidase prevent the accumulation of H_2O_2 within the cell by converting it to H_2O and O_2.[33]

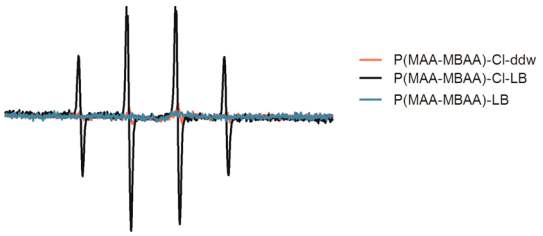

Figure 8. P(MAA-MBAA)-Cl NPs provoke formation of hydroxyl radicals. EPR spectrum of the DMPO-OH adducts formed upon mixing P(MAA-MBAA)-Cl NPs with LB medium (black line) or distilled water (red line). The blue line represents P(MAA-MBAA) NPs mixed with LB media.

Accordingly, *sodA* is considered to be a key enzyme in *E. coli* oxidative stress response. The *micF* gene encodes a nontranslated 93 nt antisense RNA that binds the mRNA of the outer membrane porin protein (OmpF), triggering OmpF degradation and hence representing a negative regulator.[34] OmpF forms pores at the outer cell membrane, allowing the passive diffusion of small hydrophilic molecules across the membrane.[35] Regulation of outer membrane permeability critically influences survival of the bacteria in response to environmental stress. Indeed, various environmental factors have been shown to be involved in MicF-mediated reduction of OmpF levels, such as oxidative stress,[36] nutrient depletion,[37,38] and increased osmolarity.[37,39]

Since activation of these two reporter strains is associated with oxidative stress, we carried out electron paramagnetic resonance (EPR) measurements to determine directly whether the chlorinated NPs generate ROS using 5,5-dimethyl-1-pyrroline-*N*-oxide (DMPO) to trap oxygen-centered free radicals. The DMPO spin trap reacts with ROS, such as hydroxyl radicals or superoxide anion radicals, to produce the spin adducts DMPO-OH or DMPOOH, respectively. The DMPO-OH is a relatively stable paramagnetic species with a characteristic EPR signal of 1:2:2:1 quartet.[40] We observed a typical EPR spectrum of DMPO-OH, giving rise to four resolved peaks (Figure 8), suggesting the formation of hydroxyl radicals (•OH). Of note, these radicals were formed only following exposure of the nanosized P(MAA-MBAA)-Cl to organic reagents, such as LB media, and not when the chlorinated NPs were suspended in water (Figure 8), revealing a target-specific mode of action. To further elucidate with what components in the LB medium the chlorinated NPs interact to generate the hydroxyl radicals, each of the materials found within this growth medium (*i.e.*, Tryptone, yeast extract, and NaCl) was exposed to the P(MAA-MBAA)-Cl NPs. Only the Tryptone and the yeast extract triggered ROS formation by the NPs as opposed to NaCl, which did not interact with the particles (Supporting Information, Figure S5), emphasizing the specificity of the charged NPs toward organic materials. This remarkable specificity is not exhibited by NaOCl, as we (data not shown) and others[41] have demonstrated the generation of free radicals upon mixing NaOCl with water. Similar to NaOCl, other NPs (*e.g.*, metal oxides) have been shown to generate ROS in water suspensions,[22,25] emphasizing that this specific activation in organic medium represents a unique and beneficial property of the chlorinated NPs. We surmise that the ROS are generated directly or indirectly by the oxidative chlorine attached to the NPs because non-chlorinated NPs did not provoke the formation of hydroxyl radicals (Figure 8). This model is in line with our earlier observations that the chlorinated adducts are released only upon incubation with organic agents (Figure 5) and not when suspended in water.[27] It is important to note that the charged NPs are capable of killing bacteria suspended in water (Supporting Information, Figure S4), as the chlorinated NPs can exert toxicity *via* a direct transfer of the oxidative chlorine to a bacterial associated component.[42] Therefore, it seems like the P(MAA-MBAA)-Cl NPs can kill bacteria both in the presence of organic substances (*via* ROS generation or through a transfer of the Cl^+ to bacteria) and in the presence of water only upon addition of bacteria.

The •OH free radicals are extremely toxic and notorious for their ability to cause cellular damages, including DNA damage and oxidation of lipids and amino acids in proteins.[43] Thus, the formation of ROS by P(MAA-MBAA)-Cl provides a mechanistic basis whereby these NPs exert detrimental effects. The proposed relationship between ROS production and bacterial killing is corroborated by our finding that lower concentrations of chlorinated NPs are associated with reduced production of the DMPO-OH quartet signal and, in turn, partial killing of bacteria (Figure 9). In fact, low concentrations (1.25 mM) of P(MAA-MBAA)-Cl that do not kill the bacteria (Figure 9A) hardly trigger formation of ROS (Figure 9B). In summary, the Cl^+-charged NPs promote formation of ROS, which triggers the oxidative-type stress response and, ultimately, results in cell death.

To further corroborate that the chlorinated NPs trigger formation of •OH and that these radicals are the cause for the antibacterial activity imparted by the NPs, we exploited dimethyl sulfoxide (DMSO), *N*-acetyl cysteine (NAC), and ascorbic acid (AA) as potent hydroxyl radical scavengers, serving as an established means of mitigating the deleterious effects of •OH. In line with our model that mixing P(MAA-MBAA)-Cl NPs with organic reagents leads to ROS formation, DMSO addition reduced the levels of DMPO-OH by 60%, while NAC and AA completely abrogated the formation of DMPO-OH (Figure 10A). In light of these results, the effect of these antioxidants on the chlorinated NPs' antibacterial activity was examined. While the P(MAA-MBAA)-Cl NPs killed both *E. coli* (Figure 10B) and *S. aureus* (Figure 10C) in the presence of LB after 15 min,

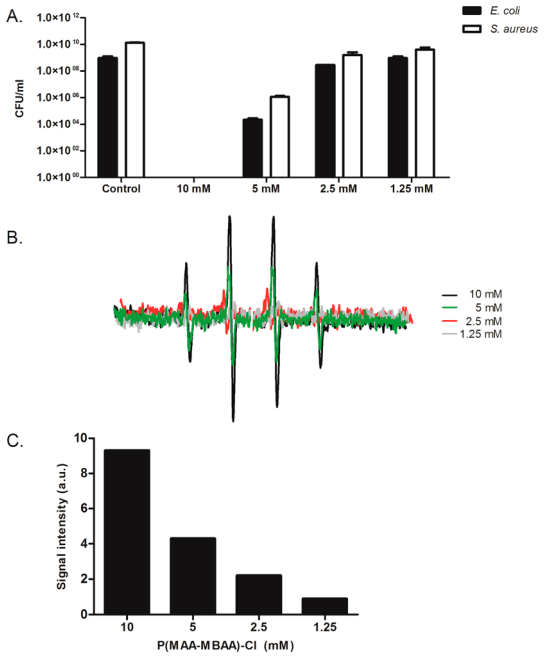

Figure 9. Antibacterial activity of P(MAA-MBAA)-Cl NPs is proportional to the quantity of the radicals formed. (A) CFU/mL of *E. coli* and *S. aureus* exposed to 1.25−10 mM of P(MAA-MBAA)-Cl NPs or to distilled water (negative control) for 24 h at 37 °C. (B) EPR spectrum of the DMPO adducts formed upon mixing LB medium with increasing concentrations of oxidative chlorine bound to P(MAA-MBAA)-Cl NPs (1.25−10 mM). (C) Quantification of ROS formed in response to increasing concentrations of the chlorinated NPs (calculated from double integration of the DMPO-OH spin adduct quartet).

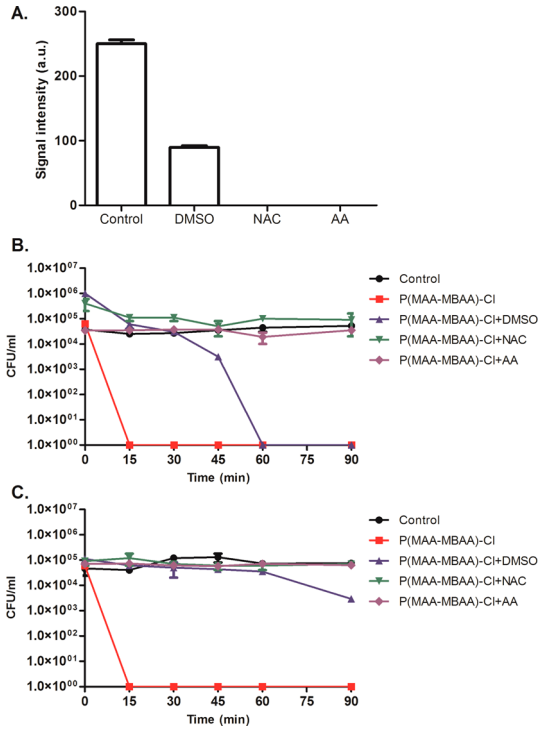

Figure 10. (A) ROS formation upon mixing P(MAA-MBAA)-Cl NPs with LB without (*i.e.*, control) or with addition of either 10% DMSO, 10 mM NAC, or 10 mM AA. Killing kinetic curves of *E. coli* (B) and *S. aureus* (C) in the presence of P(MAA-MBAA)-Cl NPs that were preincubated with either DDW (*i.e.*, control) or the indicated antioxidants for 1 h before adding the relevant bacteria.

preincubation of the chlorinated NPs with either NAC or AA prior to the addition of bacteria abolished the killing properties of the NPs (Figure 10B,C). Of note, DMSO was less efficient at mitigating bacterial cell death, as after 60 min, *E. coli* bacteria were eliminated, while at 90 min, the P(MAA-MBAA)-Cl NPs started to affect the growth of *S. aureus* (Figure 10B,C), which was also reflected by the capacity of DMSO to compromise but not eliminate the charged NPs' ability to mediate hydroxyl radical formation (Figure 10A).

P(MAA-MBAA)-Cl NPs Specifically Target Bacteria and Mark Them for Destruction. To investigate in more detail the mechanisms underlying the antibacterial activity of P(MAA-MBAA)-Cl NPs, we conducted TEM to examine if the NPs exert morphological effects on the bacteria. We did not observe any detectable morphological changes within *S. aureus* bacteria following treatment with the chlorinated NPs for 1.5 h (Figure 11A), which corresponds to the time needed to kill 10^9 CFU/mL of these bacteria (data not shown). However, we did observe the formation of very organized structures of particles around the bacteria, specifically accumulating at the cell wall and encircling it like "necklaces" (Figure 11A). Remarkably, these particles were not observed in the extracellular space, suggesting a specific interaction of these particles with the bacteria. Of note, these layers of particles did not surround cells treated with distilled water (data not shown) or non-chlorinated NPs (Figure 11A), suggesting that the oxidative chlorine on the NPs is responsible for this unusual phenomenon. Moreover, the particles decorated the bacteria at 15 min, revealing not only a specific interaction with the bacterial cells but also a rapid one (Figure 11B). We quantified the proportion of cells marked with these particles and found that 100% of the cells exhibited these structures after only 15 min ($n = 300$), although some cells were encircled with less particles than others.

One interpretation of the data is that these particles are the P(MAA-MBAA)-Cl NPs themselves. Another option is that cellular material is secreted by the bacteria due to the stress imposed by the chlorinated NPs, although the latter is less likely due to the rapid appearance of the particles on the cell surface. Moreover, cells treated with bleach did not exhibit this unusual phenomenon (Figure S6), further supporting our hypothesis that the chlorinated NPs are the ones tagging the bacteria. To differentiate between these options, we synthesized NPs 6 times larger than those utilized throughout this study, that is, 190 ± 20 nm as opposed to 27 ± 3 nm hydrodynamic diameter according to dynamic light scattering measurements (Figure 12A). The cryo-TEM images presented in Figure 12B illustrate the difference in dry size; the small

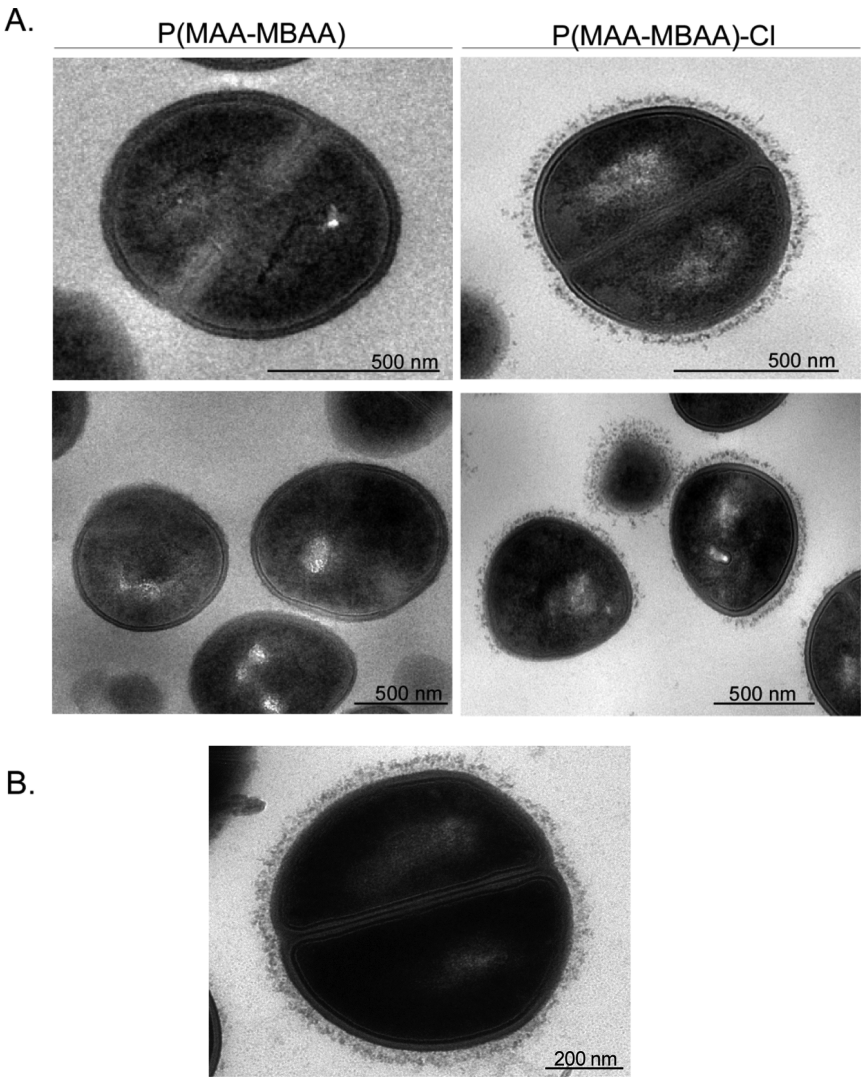

Figure 11. Transmission electron microscopy of *S. aureus* bacteria. (A) *S. aureus* were treated with either P(MAA-MBAA) NPs or their chlorinated counterparts for 1.5 h. (B) TEM micrographs of *S. aureus* treated with the P(MAA-MBAA)-Cl NPs for 15 min.

NPs are about 3−15 nm, whereas the large NPs are mostly aggregates of 100−200 nm. As presented in Figure 12C, bacteria treated with the bigger NPs were indeed surrounded by larger particles, the size of which matched the TEM measurements of NPs alone (Figure 12B). Notably, although the larger P(MAA-MBAA)-Cl NPs associated mainly with the bacterial cells, there were some aggregates in the extracellular environment unlike our observations of the small NPs, which were only observed surrounding the bacteria. This finding suggests that the small NPs may be more target-specific and, therefore, superior for bacterial killing. These data support our model that the chlorinated NPs specifically interact with the bacteria *via* oxidative chlorine release and inflict toxic effects on the bacteria that are trapped within these nanocages. This nanocaging was further illustrated *via* SEM images that show the NPs' 3D morphology (Supporting Information, Figure S7). There are several reports showing that other types of NPs can interact and penetrate cells,[22,24,44,45] but to the best of our knowledge, this is the first documentation of specific and organized interaction of NPs with bacteria, without any traces left in the extracellular environment. These data suggest that chlorinated NPs have a uniquely strong tendency to adhere and circle the bacterial cell wall rather than aggregate. Moreover, the observation that every bacterium was marked with chlorinated NPs further emphasizes their potency as an antibacterial agent. Of note, no pronounced appearance of NPs around *E. coli* was detected (Supporting Information, Figure S8), which could be explained by the different cell wall composition of Gram-negative *versus* Gram-positive bacteria.

In addition, we examined the ability of the charged NPs to target mammalian cells, using the osteosarcoma cell line Saos-2. As can be seen in Figure S9, no particles were observed around the Saos-2 cells, whether the P(MAA-MBAA) or the P(MAA-MBAA)-Cl NPs were applied. We conclude that *S. aureus* bacteria

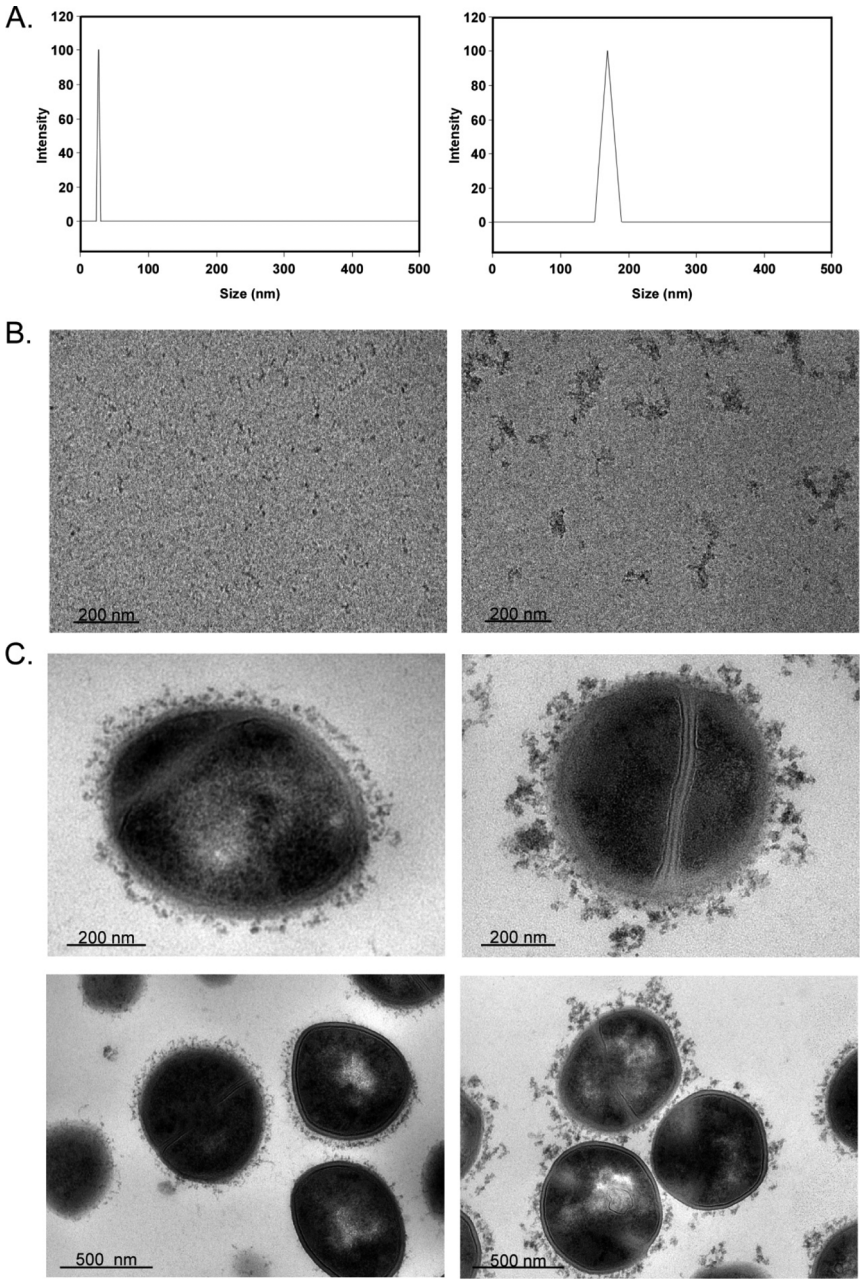

Figure 12. Hydrodynamic size histogram (A) and cryo-TEM images of the P(MAA-MBAA)-Cl NPs synthesized at two different sizes, *i.e.*, small (left) and big (right). (C) TEM micrographs of *S. aureus* bacteria treated for 1.5 h with the chlorinated NPs of two different sizes.

are specifically marked for destruction by the chlorinated NPs, which unload their oxidative Cl cargo and eliminate the bacteria.

To determine if the gathering of the chlorinated NPs at the cell wall of *S. aureus* requires energy, the cells were either preincubated at 4 °C for 2 h or thermally killed (*i.e.*, boiled for 10 min) before adding the NPs. As shown in Figure S10, inactivating the metabolic state of *S. aureus* or killing it did not abrogate the formation of the structures around the cells, suggesting neither energy nor cellular proteins/enzymes are required for this interaction to occur. Moreover, using the antioxidant DMSO did not abolish the bacterial decoration by the P(MAA-MBAA)-Cl NPs, suggesting ROS formation is not a prerequisite for this tagging either (Figure S10). Nevertheless, when the NPs were mixed with bacteria suspended in water, the cells were barley marked with the particles (Figure S11), which may imply that some component found in LB is mediating the interaction between the bacteria and the NPs. Of importance, the zeta-potential of the NPs becomes positive when LB is added to the particles' suspension, that is, 1.59 mV (as opposed to the negative value received from the suspension itself). This may suggest that the attraction of the NPs to the bacteria is favored when LB is added due to the positively charged

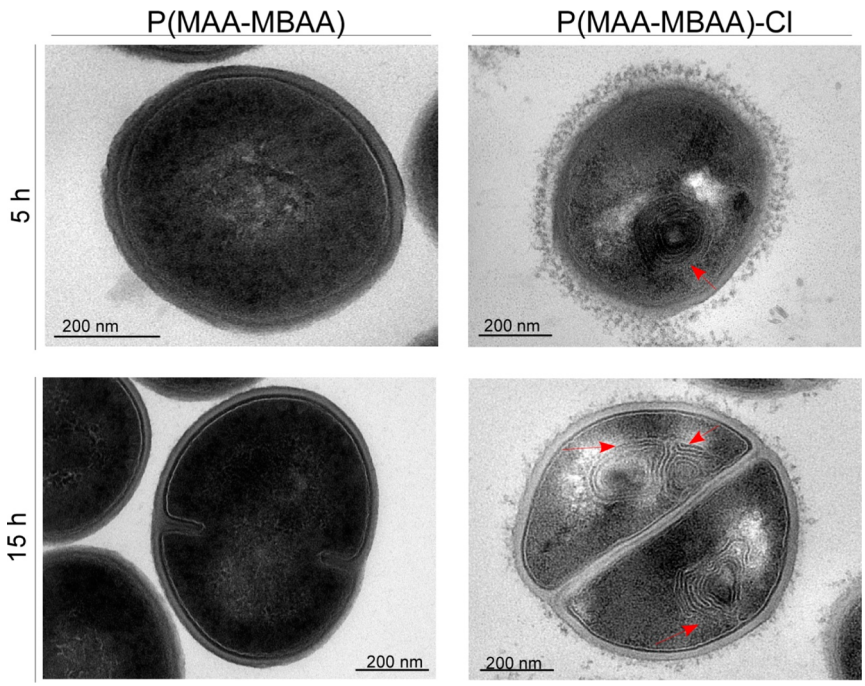

Figure 13. P(MAA-MBAA)-Cl NPs trigger morphological changes within the bacteria. *S. aureus* were treated with either P(MAA-MBAA) NPs or chlorinated counterparts for 5 or 15 h. The red arrows designate membrane constructs.

NPs that are now attracted to the negatively charged bacterial surface.

Since there were no noticeable morphological changes following incubation with P(MAA-MBAA)-Cl NPs for 1.5 h, we extended the incubation to 5 and 15 h. After 5 and 15 h of incubation with the chlorinated nanosized agents, membrane "snail-like" structures were observed to accumulate within the *S. aureus* cells (Figure 13). This phenomenon was not detected within cells treated with non-chlorinated NPs (Figure 13) or distilled water (data not shown), suggesting that the oxidative chlorine provoked directly or indirectly the formation of these tightly packed intracellular membrane structures. Future work is required to further characterize the nature of these structures.

CONCLUSIONS

This study aimed to decipher the antibacterial mechanism of *N*-halamine NPs, loaded with oxidative chlorine (*i.e.*, P(MAA-MBAA)-Cl). We demonstrate that chlorinated NPs possess high stability when exposed to rich organic materials and can withstand consecutive bacterial loading cycles, unlike NaOCl ("bleach"), one of the most commercially used sanitizers today. This stability is associated with a slower release of oxidative chlorine as compared to NaOCl. Taking advantage of bioreporter strains that respond to specific stresses, we uncovered that the chlorinated NPs trigger oxidative stress and, therefore, surmised that the mechanism underlying the toxicity likely involves ROS. We proceeded to validate this model using EPR measurements and demonstrated that hydroxyl radicals are formed specifically when P(MAA-MBAA)-Cl NPs are mixed with organic materials and not when suspended in water, a specificity that is not demonstrated by bleach. Furthermore, we found using electron microscopy that the chlorinated NPs form symmetrical structures around *S. aureus* bacteria, specifically targeting and evenly surrounding the entire cell, marking it for execution. The remarkable specificity of chlorinated nanomaterials, namely, that oxidative chlorine is released and ROS generated only when encountering organic substances, combined with the efficacy and unique targeting, makes this agent an ideal antibacterial candidate for industrial applications and medical devices.

METHODS

Synthesis and Characterization of the Cross-Linked P(MAA-MBAA) NPs. P(MAA-MBAA) NPs were synthesized *via* surfactant-free dispersion copolymerization of the monomer methacrylamide and the cross-linking monomer *N*,*N*-methylenebis(acrylamide) in water as a continuous phase, as previously described.[27] In brief, P(MAA-MBAA) NPs of either 27 ± 3 or 170 ± 20 nm hydrodynamic diameter were formed by dissolution of 4.4 g of MAA, 3.6 g of MBAA (2% w/v total monomers), and 240 mg of potassium persulfate in 400 mL of distilled water. The 1 L round-bottom flask containing this solution was stirred for 1 h with a mechanical stirrer (200 rpm) at 100 or 80 °C to obtain NPs at sizes of either 27 ± 3 or 170 ± 20 nm hydrodynamic diameters, respectively. To achieve a soluble polymer, the same procedure was carried out, just without the cross-linking monomer MBAA. The MAA and MBAA residues were subsequently removed from

the NP aqueous dispersion by extensive dialysis against water. The dried P(MAA-MBAA) NPs were obtained by lyophilization and were verified by solid-state NMR.

MAA Monomer. ^{1}H NMR (solid): δ 1.93 (s, 3H, Me), 5.12 (s, 1H, vinyl), 5.91(s, 1H, vinyl), 8.38 (br s, 2H, NH_2). ^{13}C NMR (solid): δ 19.80 (Me), 122.95 (CH_2—vinyl), 138.82 (C—vinyl), 171.63 (C═O).

P(MAA-MBAA) NPs. ^{1}H NMR (solid): δ 1.83 (br s, 12H, CH_2CHCH_3 of MMA and 2 × CH_2CH-C of MBBA), 4.77 (s, 2H, N—CH_2—N), 8.12 (br s, 4H, NH_2 and $NHCH_2NH$). ^{13}C NMR (solid): δ 18.73 (C—CH_2—C), 21.15 (Me and CH_2—CH_2—C═O), 41.87 (Me—C—C═O), 45.72 (NH—CH_2—NH), 180.21 (C═O). The percent conversion (polymerization yield) of the monomers to P(MAA-MBAA) NPs was calculated using the following expression:

$$\text{polymerization yield (wt \%)} = \frac{W_{P(MAA-MBAA)}}{W_{(MAA+MBAA)}} \times 100$$

where $W_{P(MMA-MBAA)}$ is the weight of the obtained dried P(MAA-MBAA) NPs and $W_{(MAA+MBAA)}$ is the initial weight of the monomers MAA and MBAA. Both the hydrodynamic diameter and the size distribution of the NPs dispersed in water were measured at room temperature with a particle analyzer, model NANOPHOX (Sympatec GmbH, Germany). The size of the dried particles was evaluated and imaged with a cryogenic transmission electron microscope. Samples for cryo-TEM were prepared by placing a droplet of the solution on a TEM grid coated with holey carbon film (lacey carbon, 300 mesh, Ted Pella, Inc.), followed by automatic blotting of the excess liquid. The specimen was vitrified by rapid plunging into liquid ethane precooled with liquid nitrogen in a controlled environment vitrification system (Leica EM GP). The vitrified samples were transferred to a cryospecimen holder (Gatan model 626) and examined at −178 °C in low-dose mode. Imaging was carried out using FEI Tecnai 12 G^2 equipped with Gatan 794 CCD camera and operated at 120 kV. The zeta-potential measurements were performed with a Wallis zeta-potential analyzer (Cordouan, France).

Chlorination of the P(MAA-MBAA) NPs. Sodium hypochlorite (Sigma-Aldrich) aqueous solution (5 mL, 4% w/v) was added to the aqueous dispersion of the P(MAA-MBAA) NPs (5 mL, 15 mg/mL), and the mixture was shaken at room temperature for 1 h. Excess sodium hypochlorite was removed from the P(MAA-MBAA)-Cl NP dispersion by extensive dialysis against water. The bound Cl content of the P(MAA-MBAA)-Cl NPs was determined either by adding sodium iodide and measuring the formed color spectrophotometrically at 292 and 350 nm[46,47] or by iodometric/thiosulfate titration according to the literature[48] using the following expression:

$$Cl^+(mM) = \frac{N \times V \times 1000}{2}$$

where N is the normality (equiv/L) and V is the volume (L) of the titrated sodium thiosulfate solution. The same procedure was done for the soluble polymer. In all of the experiments, the oxidative chlorine concentration on the NPs or NaOCl was set at 0.011 M unless indicated otherwise.

NMR Analysis. Solid-state NMR experiments were performed on a Bruker Advance III 500 MHz narrow-bore spectrometer, using a 4 mm double-resonance magic angle spinning (MAS) probe. ^{13}C CPMAS experiments were carried out at a spinning rate of 8 kHz, using a 2.8 μs 1H 90° pulse, 2k data points, and a 2 ms ramped CP period. Proton decoupling using the SPINAL composite pulse sequence at a field of 100 kHz was used during acquisition with a 3 s recycle delay between acquisitions. Chemical shifts were given with respect to adamantane (38.55, 29.497 ppm).

XRD. Powder X-ray diffraction patterns were recorded using an X-ray diffractometer (model D8 Advance, Bruker AXS) with Cu Kα radiation.

Cell Cultures and Growth Conditions. In all experiments, both *Escherichia coli* C600 and *Staphylococcus aureus* FRF1169 were grown overnight at 37 °C under agitation (250 rpm) in LB (Difco) growth medium. The human osteosarcoma cell line Saos-2 (ATCC #HTB-85) was maintained in Dulbecco's minimum essential medium supplemented with 10% heat-inactivated fetal bovine serum, 100 IU/mL penicillin, 100 mg/mL streptomycin, and 2 mM L-glutamine; all of these reagents were purchased from Biological Industries (Bet Haemek, Israel).

Antimicrobial Activity of P(MAA-MBAA)-Cl NPs, PMAA-Cl, and NaOCl. The cell density of *E. coli* and *S. aureus* grown overnight was normalized to 2 × 10^5 cells per milliliter in a 2-fold concentrated LB medium. Then, the bacteria were incubated overnight at 37 °C under agitation (250 rpm) with equivalent volumes of either NaOCl or P(MAA-MBAA)-Cl NPs or the non-nanometric PMAA-Cl. Bacteria shaken with water served as a negative control. Serial dilutions were carried out and the cells spotted onto LB agar plates, which were incubated at 37 °C for 20 h. Cell growth was monitored and determined by a viable cell count.

Antimicrobial Activity Assay of P(MAA-MBAA)-Cl NPs and NaOCl. The antimicrobial activity of P(MAA-MBAA)-Cl NPs and NaOCl was evaluated by determining the minimum inhibitory concentration values (with the lowest oxidative chlorine concentration on the NPs or the NaOCl) at which no bacterial growth was visible following incubation with either *E. coli* or *S. aureus*. The stock solutions of P(MAA-MBAA)-Cl NPs and NaOCl were each diluted in 2-fold serial dilutions in a 96-well plate (Griener Bio-one) with oxidative chlorine concentrations ranging from 0.01 M to 0.08 mM in LB medium. Each well contained 10^5 CFU/mL of either *E. coli* or *S. aureus*; bacteria treated with P(MAA-MBAA) NPs or untreated served as negative controls. The bacterial growth was monitored *via* absorbance measurements at OD_{595}, utilizing a microplate reader (Synergy 2, BioTek Instruments). All experiments were conducted in triplicate.

Incubation of P(MAA-MBAA)-Cl NPs and NaOCl with Consecutive Bacterial Loading Cycles. The cell density of *E. coli* and *S. aureus* grown overnight was normalized to 2 × 10^5 cells per milliliter in a 2-fold concentrated LB medium; then the bacteria were treated for 1 h at 37 °C under agitation (250 rpm) with equivalent volumes of either NaOCl or P(MAA-MBAA)-Cl NPs. Bacteria shaken with water served as a negative control. After 1 h of incubation, aliquots were collected and diluted serially 10-fold before spotting onto LB agar plates. After an overnight incubation at 37 °C, the CFUs were counted and used to determine cell survival. Immediately after each aliquot was removed, newly prepared bacteria were added for another hour to each of the tubes to achieve a final concentration of 10^5 CFU/mL.

Determining the Stability of the P(MAA-MBAA)-Cl NPs and NaOCl in Organic-Rich Media. One milliliter of either DDW, NaOCl, or P(MAA-MBAA)-Cl NPs was mixed with 1 mL of 2-fold concentrated LB medium and incubated for 3, 5, or 24 h. Then, *E. coli* or *S. aureus* was added to each of the solutions, reaching a final concentration of 10^5 CFU/mL, and the mixture was agitated for either 3 or 24 h. At the indicated time points, samples were taken for cell viability determination and the solutions were reloaded with freshly prepared bacteria. The experiment was continued until the reagents were no longer capable of evincing toxic effects on the tested bacteria.

Kinetics of Oxidative Chlorine Release from the Charged NPs and NaOCl in the Presence of Organic-Rich Media. Equal volumes of NaOCl or P(MAA-MBAA)-Cl NPs were incubated with equivalent volumes of 2-fold concentrated LB medium. The precise concentration of the oxidative chlorine found on the two reagents was determined at different time intervals *via* quenching with sodium iodide followed by spectrophotometry (Amersham Bioschiences) measurements at wavelengths of 292 and 350 nm, as previously described.[46,47]

Bacterial Killing Kinetics in the Presence of P(MAA-MBAA)-Cl NPs and NaOCl. Cultures of *E. coli* and *S. aureus* bacteria grown overnight were diluted in fresh 2-fold concentrated LB medium or water to obtain stock solutions with a final working concentration of 10^5 CFU/mL. Then, *E. coli* and *S. aureus* bacteria were grown with either P(MAA-MBAA)-Cl NPs or NaOCl under continuous agitation (250 rpm). Bacteria grown with distilled water or P(MAA-MBAA) NPs served as negative controls. At various time points, 100 μL samples were taken from each tube and transferred into the first row wells of a 96-well plate containing 20 μL of 0.1 N thiosulfate. The latter was added to quench the remaining chlorine on the P(MAA-MBAA)-Cl NPs and NaOCl, thus terminating the sterilization process. Serial dilutions were carried out

and the cells spotted onto LB agar plates, which were incubated at 37 °C for 20 h. Cell growth was monitored and determined by a viable cell count.

Biosensor Bacteria Screening Assay. A panel of seven modified *E. coli* strains[29−31] was utilized for this study (Table 2). Each strain contains a multicopy plasmid in which the promoter of interest is fused to the *Vibrio fischeri luxCDABE* genes, such that promoter activation, for example, by toxic stress, drives the synthesis of luciferase, ultimately resulting in bioluminescence. All strains were handled alike. Bacteria were grown overnight at 37 °C under agitation (250 rpm) in LB that was supplemented with 100 mg/mL ampicillin to guarantee plasmid maintenance. The following day, the culture was diluted 1:100 with fresh LB media and incubated at 30 °C under agitation (200 rpm) until an OD_{595} of 0.1−0.2 was reached. Then, 100 μL of either distilled water or P(MAA-MBAA)-Cl NPs or their non-chlorinated counterparts was added in triplicate to the first row of an opaque white 96-well plate (Griener Bio-one). Then all wells were filled with 100 μL of the culture, now in logarithmic phase, and 2-fold serial dilution conducted to generate oxidative chlorine concentrations ranging from 0.01 M to 0.08 mM. The plate was placed in a luminometer (in the dark), and luminescence was measured at 10 min intervals at a constant temperature (25 °C).

EPR Measurements. ROS production was detected using the EPR spin trapping technique coupled with a spin trap 5,5-dimethyl-1-pyrroline-*N*-oxide (Sigma, St. Louis, MO). Typically, the aqueous suspensions of NPs were added to DMPO (0.01 M) in the presence of equivalent volumes of either 2-fold concentrated LB medium or each of its components (Tryptone, yeast extract, NaCl) or water. Whenever indicated, the following antioxidants were added to the reaction: 10% DMSO, 10 mM *N*-acetyl cysteine and 10 mM ascorbic acid; all were purchased from Sigma. The solution was drawn into a 0.8 mm i.d. capillary quartz tube sealed at both ends with a plastic Critoseal (Thermo Fisher Scientific Inc.), which was placed into a quartz tube that in turn was placed into the EPR rectangular cavity (ER 4122SHQ). The measurements were taken using a X-band Elexsys E500 EPR spectrometer (Bruker, Karlsruhe, Germany) using the following parameters: microwave power, 20 mW; scan width, 100 G; resolution, 1024; gain, 60; sweep time, 60 s; number of scans, 2; modulation frequency, 100 kHz; modulation amplitude, 1 G. In order to compare the radical intensity, the double integration of the spin adduct signal was calculated using the Xepr 2.6b.58 acquisition version.

Bacterial Killing Kinetics of P(MAA-MBAA)-Cl NPs in the Presence of Antioxidants. Cultures of *E. coli* and *S. aureus* bacteria grown overnight were diluted in fresh 2-fold concentrated LB medium to obtain stock solutions with a final working concentration of 10^5 CFU/mL. Then, *E. coli* and *S. aureus* bacteria were grown with P(MAA-MBAA)-Cl NPs that were preincubated with either antioxidants (*i.e.*, 10% DMSO, 10 mM NAC, 10 mM AA) or water for 1 h, under continuous agitation (250 rpm). Bacteria supplemented with distilled water or the various antioxidants served as negative controls. At various time points, 100 μL samples were taken from each tube and transferred into the first row wells of a 96-well plate containing 20 μL of 0.1 N thiosulfate. The latter was added to quench the remaining chlorine on the P(MAA-MBAA)-Cl NPs and NaOCl, thus terminating the sterilization process. Serial dilutions were carried out and the cells spotted onto LB agar plates, which were incubated at 37 °C for 20 h. Cell growth was monitored and determined by a viable cell count.

Transmission Electron Microscopy of Bacterial Samples. Samples of *S. aureus* and *E. coli* cultures (10^9 CFU/mL) or the human osteosarcoma cell line Saos-2 ATCC HTB-85 were centrifuged immediately after treatment with either distilled water, P(MAA-MBAA) NPs, P(MAA-MBAA)-Cl, or NaOCl for the indicated time points. When indicated, *S. aureus* bacteria were boiled for 10 min or preincubated at 4 °C for 2 h before adding the NPs. When indicated, DMSO was incubated with the chlorinated NPs for 1 h prior to the addition of bacteria. In all of the experiments, the bacteria were suspended in LB medium unless indicated otherwise. The samples were then fixed in 2.5% glutaraldehyde/paraformaldehyde in cacodylate buffer (Electron Microscopy Sciences). The samples were washed with cacodylate buffer and fixed in 1% osmium tetraoxide. Embedding of samples was carried out according to standard protocols,[49] and 60 nm thick slices were cut with a diamond knife (LBR ultratome III). The slices were deposited on bare 200 mesh copper grids and stained with 2 wt % uranyl acetate for 5 min. Finally, the grids were dried in a desiccator and examined using a JEOL 1200Ex transmission electron microscope at 80 kV. The percentage of cells marked with the particles was calculated by taking 20 representative microscope images containing all together 300 cells.

Conflict of Interest: The authors declare no competing financial interest.

Acknowledgment. We thank Prof. Shimshon Belkin for kindly providing the biosensor bacteria. We also thank Dr. Yael Kalisman for conducting the cryo-TEM studies, and Dr. Tania Babushkin and Gila Jacobi for their assistance in the TEM experiments. We also thank Dr. Sharon Ruthstein and Dr. Gal Yerushalmi for their helpful discussion.

Supporting Information Available: Cryo-TEM image of the P(MAA-MBAA)-Cl NPs, susceptibility of NaOCl to organic materials, P(MAA-MBAA)-Cl NPs provoking formation of hydroxyl radicals in the presence of organic materials, P(MAA-MBAA)-Cl NPs killing bacteria suspended in water, scanning electron microscopy of *S. aureus* bacteria treated with P(MAA-MBAA)-Cl NPs or left untreated, transmission electron microscopy of *E. coli* bacteria treated with either P(MAA-MBAA) NPs or their chlorinated counterparts for 45 min (P(MAA-MBAA)-Cl do not need to enter the bacteria to kill them), transmission electron microscopy of Saos-2 cells treated with either P(MAA-MBAA) NPs or their chlorinated counterparts for 15 min, transmission electron microscopy of *S. aureus* bacteria treated with P(MAA-MBAA)-Cl NPs for 15 min, TEM micrographs of *S. aureus* suspended in LB or DDW followed by the addition of P(MAA-MBAA)-Cl NPs for 15 min. This material is available free of charge *via* the Internet at http://pubs.acs.org.

REFERENCES AND NOTES

1. Magiorakos, A. P.; Srinivasan, A.; Carey, R. B.; Carmeli, Y.; Falagas, M. E.; Giske, C. G.; Harbarth, S.; Hindler, J. F.; Kahlmeter, G.; Olsson-Liljequist, B.; et al. Multidrug-Resistant, Extensively Drug-Resistant and Pandrug-Resistant Bacteria: An International Expert Proposal for Interim Standard Definitions for Acquired Resistance. *Clin. Microbiol. Infect.* **2012**, *18*, 268–281.
2. Andersson, D. I.; Hughes, D. Antibiotic Resistance and Its Cost: Is It Possible Ro Reverse Resistance? *Nat. Rev. Microbiol.* **2010**, *8*, 260–271.
3. Burke, J. P. Infection Control—A Problem for Patient Safety. *N. Engl. J. Med.* **2003**, *7*, 651–656.
4. Gabriel, G. J.; Som, A.; Madkour, A. E.; Eren, T.; Tew, G. N. Infectious Disease: Connecting Innate Immunity to Biocidal Polymers. *Mater. Sci. Eng.* **2007**, *57*, 28–64.
5. Frieden, T. *Antibiotic Resistance Threats in the United States*, http://www.cdc.gov/drugresistance/threat-report-2013/index.html.
6. Kenawy, E. R.; Worley, S. D.; Broughton, R. The Chemistry and Applications of Antimicrobial Polymers: A State-of-the-Art Review. *Biomacromolecules* **2007**, *8*, 1359–1384.
7. Ringot, C.; Sol, V.; Barrière, M.; Saad, N.; Bressollier, P.; Granet, R.; Couleaud, P.; Frochot, C.; Krausz, P. Triazinyl Porphyrin-Based Photoactive Cotton Fabrics: Preparation, Characterization, and Antibacterial Activity. *Biomacromolecules* **2011**, *12*, 1716–1723.
8. Padmanabhuni, R. V.; Luo, J.; Cao, Z.; Sun, Y. Preparation and Characterization of *N*-Halamine-Based Antimicrobial Fillers. *Ind. Eng. Chem. Res.* **2013**, *51*, 5148–5156.
9. Kocer, H. B.; Cerkez, I.; Worley, S. D.; Broughton, R. M.; Huang, T. S. *N*-Halamine Copolymers for Use in Antimicrobial Paints. *ACS Appl. Mater. Interfaces* **2011**, *3*, 3189–3194.
10. Lauten, S. D.; Sarvis, H.; Wheatley, W. B.; Williams, D. E.; Mora, E. C.; Worley, S. D. Efficacies of Novel *N*-Halamine Disinfectants Against *Salmonella* and *Pseudomonas* Species. *Appl. Environ. Microbiol.* **1992**, *58*, 1240–1243.

11. Worley, S. D.; Williams, D. E.; Crawford, R. A. Halamine Water Disinfectants. *Crit. Rev. Environ. Controll* **1988**, *18*, 133–175.
12. Huang, Z.; Jiang, X.; Guo, D.; Gu, N. Controllable Synthesis and Biomedical Applications of Silver Nanomaterials. *J. Nanosci. Nanotechnol.* **2011**, *11*, 9395–9408.
13. Navarro, E.; Piccapietra, F.; Wagner, B.; Marconi, F.; Kaegi, R.; Odzak, N.; Sigg, L.; Behra, R. Toxicity of Silver Nanoparticles to *Chlamydomonas reinhardtii*. *Environ. Sci. Technol.* **2008**, *42*, 8959–8964.
14. Lok, C.; Ho, C.; Chen, R.; He, Q.; Yu, W.; Sun, H.; Tam, P. K.; Chiu, J.; Che, C. Proteomic Analysis of the Mode of Antibacterial Action of Silver Research Articles. *J. Proteome Res.* **2006**, *5*, 916–924.
15. Li, C.; Wang, X.; Chen, F.; Zhang, C.; Zhi, X.; Wang, K.; Cui, D. The Antifungal Activity of Graphene Oxide-Silver Nanocomposites. *Biomaterials* **2013**, *34*, 3882–3890.
16. Wei, L.; Tang, J.; Zhang, Z.; Chen, Y.; Zhou, G.; Xi, T. Investigation of the Cytotoxicity Mechanism of Silver Nanoparticles *in Vitro*. *Biomed. Mater.* **2010**, *5*, 1–6.
17. Asharani, P. V.; Low, G.; Mun, K.; Hande, M. P.; Valiyaveettil, S. Cytotoxicity and Genotoxicity of Silver Nanoparticles in Human Cells. *ACS Nano* **2009**, *3*, 279–290.
18. Benn, T. M.; Westerhoff, P. Nanoparticle Silver Released into Water from Commercially Available Sock Fabrics. *Environ. Sci. Technol.* **2008**, *42*, 4133–4139.
19. Phan, T. N.; Buckner, T.; Sheng, J.; Baldeck, J. D.; Marquis, R. E. Physiologic Actions of Zinc Related to Inhibition of Acid and Alkali Production by Oral Streptococci in Suspensions and Biofilms. *Oral Microbiol. Immunol.* **2004**, *19*, 31–38.
20. Hernández-Sierra, J. F.; Ruiz, F.; Pena, D. C. C.; Martínez-Gutiérrez, F.; Martínez, A. E.; Guillén, A. D. J. P.; Tapia-Pérez, H.; Castañón, G. M. The Antimicrobial Sensitivity of *Streptococcus mutans* to Nanoparticles of Silver, Zinc Oxide, and Gold. *Nanomedicine* **2008**, *4*, 237–240.
21. Ren, G.; Hu, D.; Cheng, E. W. C.; Vargas-Reus, M. A.; Reip, P.; Allaker, R. P. Characterisation of Copper Oxide Nanoparticles for Antimicrobial Applications. *Int. J. Antimicrob. Agents* **2009**, *33*, 587–590.
22. Applerot, G.; Lellouche, J.; Lipovsky, A.; Nitzan, Y.; Lubart, R.; Gedanken, A.; Banin, E. Understanding the Antibacterial Mechanism of CuO Nanoparticles: Revealing the Route of Induced Oxidative Stress. *Small* **2012**, *8*, 3326–3337.
23. Applerot, G.; Abu-Mukh, R.; Irzh, A.; Charmet, J.; Keppner, H.; Laux, E.; Guibert, G.; Gedanken, A. Decorating Parylene-Coated Glass with ZnO Nanoparticles for Antibacterial Applications: A Comparative Study of Sonochemical, Microwave, and Microwave-Plasma Coating Routes. *ACS Appl. Mater. Interfaces* **2010**, *2*, 1052–1059.
24. Lellouche, J.; Kahana, E.; Elias, S.; Gedanken, A.; Banin, E. Antibiofilm Activity of Nanosized Magnesium Fluoride. *Biomaterials* **2009**, *30*, 5969–5978.
25. Malka, E.; Perelshtein, I.; Lipovsky, A.; Shalom, Y.; Naparstek, L.; Perkas, N.; Patick, T.; Lubart, R.; Nitzan, Y.; Banin, E.; et al. Eradication of Multi-drug Resistant Bacteria by a Novel Zn-Doped CuO Nanocomposite. *Small* **2013**, *9*, 4069–4076.
26. Kang, S.; Pinault, M.; Pfefferle, L. D.; Elimelech, M. Single-Walled Carbon Nanotubes Exhibit Strong Antimicrobial Activity. *Langmuir* **2007**, *23*, 8670–8673.
27. Gutman, O.; Natan, M.; Banin, E.; Margel, S. Characterization and Antibacterial Properties of *N*-Halamine-Derivatized Cross-Linked Polymethacrylamide Nanoparticles. *Biomaterials* **2014**, *35*, 5079–5087.
28. Rutala, W. A.; Weber, D. J. Uses of Inorganic Hypochlorite (bleach) in Health-Care Facilities. *Clin. Microbiol. Rev.* **1997**, *10*, 597–610.
29. Yagur-Kroll, S.; Belkin, S. Upgrading Bioluminescent Bacterial Bioreporter Performance by Splitting the *Lux* Operon. *Anal. Bioanal. Chem.* **2011**, *400*, 1071–1082.
30. Kessler, N.; Schauer, J. J.; Yagur-Kroll, S.; Melamed, S.; Tirosh, O.; Belkin, S.; Erel, Y. A Bacterial Bioreporter Panel To Assay the Cytotoxicity of Atmospheric Particulate Matter. *Atmos. Environ.* **2012**, *63*, 94–101.
31. Yagur-Kroll, S.; Bilic, B.; Belkin, S. Strategies for Enhancing Bioluminescent Bacterial Sensor Performance by Promoter Region Manipulation. *Microb. Biotechnol.* **2010**, *3*, 300–310.
32. Fridovich, I. Superoxide Radical and Superoxide Dismutases. *Annu. Rev. Biochem.* **1995**, *64*, 97–112.
33. Hassan, H. M.; Fridovich, I. Regulation of the Synthesis of Catalase and Peroxidase in *Escherichia coli**. *J. Biol. Chem.* **1978**, *253*, 6445–6450.
34. Delihas, N.; Forst, S. *micF*: An Antisense RNA Gene Involved in Response of *Escherichia coli* to Global Stress Factors. *J. Mol. Biol.* **2001**, *313*, 1–12.
35. Nikaido, H. Porins and Specific Channels of Bacterial Outer Membranes. *Mol. Microbiol.* **1992**, *6*, 435–442.
36. Chou, J. H.; Greenberg, J. T.; Demple, B. Posttranscriptional Repression of *Escherichia coli* OmpF Protein in Response to Redox Stress: Positive Control of the *micF* Antisense RNA by the *soxRS* Locus. *J. Bacteriol.* **1993**, *175*, 1026–1031.
37. Coyer, J.; Andersen, J.; Forst, S. A.; Inouye, M.; Delihas, N. *micF* RNA in *ompB* Mutants of *Escherichia coli*: Different Pathways Regulate *micF* RNA Levels in Response to Osmolarity and Temperature Change. *J. Bacteriol.* **1990**, *172*, 4143–4150.
38. Ferrario, M.; Ernsting, B. R.; Borst, D. W.; Wiese, D. E.; Ferrario, M.; Ernsting, B. R.; Borst, D. W.; Wiese, D. E.; Blumenthal, R. M.; Matthews, R. G. The Leucine-Responsive Regulatory Protein of *Escherichia coli* Negatively Regulates Transcription of *ompC* and *micF* and Positively Regulates Translation of *ompF*. *J. Bacteriol.* **1995**, *177*, 103–113.
39. Ramani, N.; Hedeshian, M.; Freundlich, M. *micF* Antisense RNA Has a Major Role in Osmoregulation of OmpF in *Escherichia coli*. *J. Bacteriol.* **1994**, *176*, 5005–5010.
40. Makino, K.; Hagiwara, T.; Murakami, A. A Mini Review: Fundamental Aspects of Spin Trapping with DMPO. *Int. J. Radiat. Appl. Instrum.* **1991**, *37*, 657–665.
41. Bernofsky, C.; Bandara, R.; Hinojosa, O. Original Electron Spin Resonsance Studies of the Reaction of Hypochlorite with 5,5-Dimethyl-1-pyrroline-*N*-oxide. *Free Radicals Biol. Med.* **1990**, *8*, 231–239.
42. Hui, F. C.; Debiemme Chouvy, C. Antimicrobial *N*-Halamine Polymers and Coatings: A Review of Their Synthesis, Characterization, and Applications. *Biomacromolecules* **2013**, *14*, 585–601.
43. Farr, S. B.; Kogoma, T. Oxidative Stress Responses in *Escherichia coli* and *Salmonella typhimurium*. *Microbiol. Rev.* **1991**, *55*, 561–585.
44. Eshed, M.; Lellouche, J.; Gedanken, A.; Banin, E. A Zn-Doped CuO Nanocomposite Shows Enhanced Antibiofilm and Antibacterial Activities Against *Streptococcus mutans* Compared to Nanosized CuO. *Adv. Funct. Mater.* **2014**, *24*, 1382–1390.
45. Jiang, W.; Mashayekhi, H.; Xing, B. Bacterial Toxicity Comparison between Nano- and Micro-scaled Oxide Particles. *Environ. Pollut.* **2009**, *157*, 1619–1625.
46. Gebicki, J. M.; Guille, J. Spectrophotometric and High-Performance Chromatographic Assays of Hydroperoxides by the Iodometric Technique. *Anal. Biochem.* **1989**, *176*, 360–364.
47. Hicks, M.; Gebicki, J. M. A Spectrophotometric Method for the Determination of Lipid Hydroperoxides. *Anal. Biochem.* **1979**, *99*, 249–253.
48. Neville, J. The Infrared and Raman Spectra and Structure of Acrylamide. *J. Mol. Spectrosc.* **1961**, *6*, 205–214.
49. Croft, S. Electron Microscopy Methods and Protocols. *Methods Mol. Biol.* **1999**, 117.